ORCID profiles: A.B., 0000-0002-0409-2497; M.B., 0000-0002-0400-1954; A.T., 0000-0002-7308-7317; H.M.-T., 0000-0003-1602-7534.

Correspondence: Hélène Moins-Teisserenc, INSERM UMR-1160, Institut Universitaire d'Hématologie, Hôpital Saint Louis, 1 av. Claude Vellefaux, 75010 Paris, France; e-mail: helene.moins@univ-paris-diderot.fr.

References

1. Willemze R, Jaffe ES, Burg G, et al. WHO-EORTC classification for cutaneous lymphomas. *Blood*. 2005;105(10):3768-3785.
2. Olsen E, Vonderheid E, Pimpinelli N, et al; ISCL/EORTC. Revisions to the staging and classification of mycosis fungoides and Sezary syndrome: a proposal of the International Society for Cutaneous Lymphomas (ISCL) and the cutaneous lymphoma task force of the European Organization of Research and Treatment of Cancer (EORTC). *Blood*. 2007;110(6):1713-1722.
3. Poszepczynska-Guigné E, Schiavon V, D'Incan M, et al. CD158k/KIR3DL2 is a new phenotypic marker of Sezary cells: relevance for the diagnosis and follow-up of Sezary syndrome. *J Invest Dermatol*. 2004;122(3):820-823.
4. Klemke CD, Brade J, Weckesser S, et al. The diagnosis of Sézary syndrome on peripheral blood by flow cytometry requires the use of multiple markers. *Br J Dermatol*. 2008;159(4):871-880.
5. Hurabielle C, Thonnart N, Ram-Wolff C, et al. Usefulness of KIR3DL2 to diagnose, follow-up, and manage the treatment of patients with Sézary syndrome. *Clin. Cancer Res*. 2017;23(14):3619-3627.
6. Bagot M, Moretta A, Sivori S, et al. CD4(+) cutaneous T-cell lymphoma cells express the p140-killer cell immunoglobulin-like receptor. *Blood*. 2001;97(5):1388-1391.
7. Wechsler J, Bagot M, Nikolova M, et al. Killer cell immunoglobulin-like receptor expression delineates in situ Sézary syndrome lymphocytes. *J Pathol*. 2003;199(1):77-83.
8. Ortonne N, Le Gouvello S, Mansour H, et al. CD158K/KIR3DL2 transcript detection in lesional skin of patients with erythroderma is a tool for the diagnosis of Sézary syndrome. *J Invest Dermatol*. 2008;128(2):465-472.
9. Moins-Teisserenc H, Daubord M, Clave E, et al. CD158k is a reliable marker for diagnosis of Sézary syndrome and reveals an unprecedented heterogeneity of circulating malignant cells. *J Invest Dermatol*. 2015;135(1):247-257.
10. Campbell JJ, Clark RA, Watanabe R, Kupper TS. Sezary syndrome and mycosis fungoides arise from distinct T-cell subsets: a biologic rationale for their distinct clinical behaviors. *Blood*. 2010;116(5):767-771.
11. Fierro MT, Novelli M, Quaglino P, et al. Heterogeneity of circulating CD4+ memory T-cell subsets in erythrodermic patients: CD27 analysis can help to distinguish cutaneous T-cell lymphomas from inflammatory erythroderma. *Dermatology*. 2008;216(3):213-221.
12. Clark RA, Watanabe R, Teague JE, et al. Skin effector memory T cells do not recirculate and provide immune protection in alemtuzumab-treated CTCL patients. *Sci Transl Med*. 2012;4(117):117ra7.
13. Kirsch IR, Watanabe R, O'Malley JT, et al. TCR sequencing facilitates diagnosis and identifies mature T cells as the cell of origin in CTCL. *Sci Transl Med*. 2015;7(308):308ra158.
14. Gattinoni L, Lugli E, Ji Y, et al. A human memory T cell subset with stem cell-like properties. *Nat Med*. 2011;17(10):1290-1297.
15. Mueller SN, Zaid A, Carbone FR. Tissue-resident T cells: dynamic players in skin immunity. *Front Immunol*. 2014;5:332.
16. Felix J, Lambert J, Roelens M, et al. Ipilimumab reshapes T cell memory subsets in melanoma patients with clinical response. *OncoImmunology*. 2016;5(7):1136045.
17. Nagai Y, Kawahara M, Hishizawa M, et al. T memory stem cells are the hierarchical apex of adult T-cell leukemia. *Blood*. 2015;125(23):3527-3535.
18. Jones CL, Wain EM, Chu C-C, et al. Downregulation of Fas gene expression in Sézary syndrome is associated with promoter hypermethylation. *J Invest Dermatol*. 2010;130(4):1116-1125.
19. Chen L, Park S-M, Tumanov AV, et al. CD95 promotes tumour growth. *Nature*. 2010;465(7297):492-496.
20. Dulmage BO, Geskin LJ. Lessons learned from gene expression profiling of cutaneous T-cell lymphoma. *Br J Dermatol*. 2013;169(6):1188-1197.
21. Mahnke YD, Brodie TM, Sallusto F, Roederer M, Lugli E. The who's who of T-cell differentiation: human memory T-cell subsets. *Eur J Immunol*. 2013;43(11):2797-2809.
22. Watanabe R, Gehad A, Yang C, et al. Human skin is protected by four functionally and phenotypically discrete populations of resident and recirculating memory T cells. *Sci Transl Med*. 2015;7(279):279ra39.
23. Duvic M, Pinter-Brown LC, Foss FM, et al. Phase 1/2 study of mogamulizumab, a defucosylated anti-CCR4 antibody, in previously treated patients with cutaneous T-cell lymphoma. *Blood*. 2015;125(12):1883-1889.
24. Netchiporouk E, Litvinov IV, Moreau L, Gilbert M, Sasseville D, Duvic M. Deregulation in STAT signaling is important for cutaneous T-cell lymphoma (CTCL) pathogenesis and cancer progression. *Cell Cycle*. 2014;13(21):3331-3335.

DOI 10.1182/blood-2017-03-772996

To the editor:

CCL3 is a key mediator for the leukemogenic effect of *Ptpn11*-activating mutations in the stem-cell microenvironment

Lei Dong, Hong Zheng, and Cheng-Kui Qu

Division of Hematology/Oncology, Department of Pediatrics, Aflac Cancer and Blood Disorders Center, Children's Healthcare of Atlanta, Emory University, Atlanta, GA

Germ line–activating mutations of protein tyrosine phosphatase *PTPN11* (Shp2), a positive regulator of the Ras signaling pathway,[1] account for more than 50% of patients with Noonan syndrome.[2] These patients have an increased risk of developing leukemias,[3] especially juvenile myelomonocytic leukemia, a childhood myeloproliferative neoplasm (MPN). Previous studies have demonstrated that *Ptpn11* mutations induce juvenile myelomonocytic leukemia–like MPN through cell-autonomous mechanisms in an Shp2 catalytic activity-dependent manner.[4-7] We recently showed that *Ptpn11*-activating mutations in the mouse bone marrow (BM) microenvironment significantly promoted the development and progression of MPN through profound detrimental effects on hematopoietic stem cells (HSCs).[8] *Ptpn11* mutations in the BM mesenchymal stem/progenitor cells (which serve as unique sinusoidal vascular and arteriolar HSC niches[9,10]) and osteoprogenitors, but not differentiated osteoblasts or endothelial cells, caused excessive production of the CC chemokine CCL3 (also known as MIP-1α), which recruited monocytes to the area where HSCs also resided. Consequently, HSCs were hyperactivated by interleukin-1β and possibly other proinflammatory cytokines produced by monocytes, leading to exacerbated MPN and to donor cell–derived MPN after stem-cell transplantation therapy. Administration of the CCL3 receptor antagonists ameliorated MPN induced by the *Ptpn11*-mutated BM microenvironment. However, the mice were only treated and monitored for a limited time (3 weeks) with the CCL3 receptor

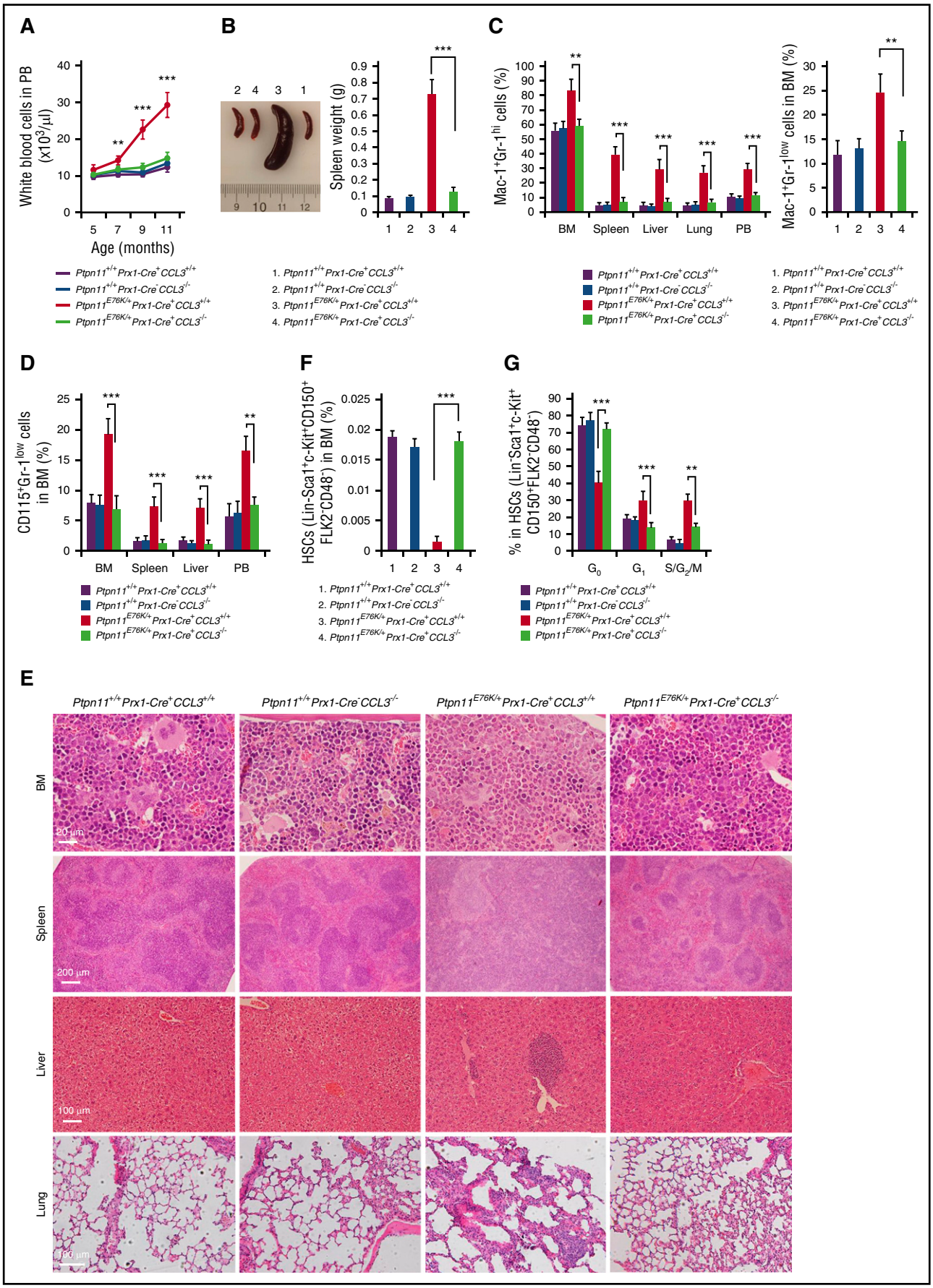

Figure 1.

antagonists. The role of CCL3 in mediating the pathogenic effects of *Ptpn11*-mutated BM stromal cells needs to be further tested. The long-term effect of CCL3 inhibition on microenvironmental *Ptpn11*-activating mutation–induced MPN has yet to be determined.

The *Ptpn11*^{E76K}-activating mutation in Prx1-expressing broad mesenchymal cells in the BM, which contain/overlap with mesenchymal stem/progenitor cells, induced MPN in *Ptpn11*$^{E76K/+}$*Prx1-Cre*$^{+}$ mice at the age of 5 to 10 months.[8] To further determine the role of CCL3 in the pathogenesis of the MPN driven by the *Ptpn11*^{E76K} mutation in the stem-cell microenvironment, we took a mouse genetic approach and examined the microenvironmental effect of the *Ptpn11*$^{E76K/+}$ mutation in the *CCL3*-knockout background. We generated *Ptpn11*$^{E76K/+}$*Prx1-Cre*$^{+}$*CCL3*$^{-/-}$ mice by crossing *Ptpn11*^{E76K} conditional knockin mice[5] with *CCL3*$^{+/-}$ mice[11] and *Prx1-Cre*$^{+}$ transgenic mice.[12] The mice were monitored for 12 to 17 months. The phenotypes of these double mutants were compared with those of *Ptpn11*$^{E76K/+}$*Prx1-Cre*$^{+}$ and *CCL3*$^{-/-}$ single-mutant mice. As expected, *Ptpn11*$^{E76K/+}$*Prx1-Cre*$^{+}$ mice developed MPN that was derived from wild-type HSCs without *Ptpn11* mutations (data not shown). These animals manifested high white blood cell counts (Figure 1A), splenomegaly (Figure 1B), elevated myeloid cells (Mac-1^{+}Gr-1^{high} and Mac-1^{+}Gr-1^{low}; Figure 1C), and monocytes (CD115^{+}Gr-1^{low}; Figure 1D) in the peripheral blood, BM, and spleen. Moreover, there was substantial infiltration of myeloid cells and monocytes in the liver and lung (Figure 1C-D). *CCL3*$^{-/-}$ mice seemed normal and indistinguishable from wild-type control littermates. No abnormalities in hematopoietic cell development were detected in CCL3 knockout mice (Figure 1A-D), suggesting that CCL3 is dispensable for steady-state hematopoiesis. Importantly, MPN phenotypes induced by the *Ptpn11*$^{E76K/+}$ mutation in Prx1-expressing BM mesenchymal cells were essentially blocked in *Ptpn11*$^{E76K/+}$*Prx1-Cre*$^{+}$*CCL3*$^{-/-}$ double-mutant mice (Figure 1A-D). Histopathological examination verified that MPN-associated phenotypes were indeed substantially attenuated in these double mutants (Figure 1E).

To further determine whether the rescue effect of *CCL3* deletion on the microenvironmental *Ptpn11* mutation–induced MPN occurred at the stem-cell level, we examined HSCs in *Ptpn11*$^{E76K/+}$*Prx1-Cre*$^{+}$*CCL3*$^{-/-}$ double-mutant mice and compared them with those in *Ptpn11*$^{E76K/+}$*Prx1-Cre*$^{+}$ single mutants. The frequency of HSCs in the BM of *Ptpn11*$^{E76K/+}$*Prx1-Cre*$^{+}$ mice was significantly decreased because of stem-cell hyperactivation and attrition as compared with that in control animals (Figure 1F). *CCL3*$^{-/-}$ mice did not show abnormalities in HSC numbers (Figure 1F). Importantly, the size of the stem-cell pool in *Ptpn11*$^{E76K/+}$*Prx1-Cre*$^{+}$*CCL3*$^{-/-}$ mice was normalized (Figure 1F). Cell-cycle analyses demonstrated that the number of quiescent HSCs in the G_0 phase decreased by half, whereas HSCs in the G_1 or $S/G_2/M$ phase doubled in *Ptpn11*$^{E76K/+}$*Prx1-Cre*$^{+}$ mice (Figure 1G), consistent with what we observed in *Ptpn11*$^{E76K/+}$*Nestin-Cre*$^{+}$ mice,[8] which also developed MPN. Moreover, aberrant HSC activation occurred before MPN was fully developed in *Ptpn11*$^{E76K/+}$*Prx1-Cre*$^{+}$ mice (supplemental Figure 1, available on the *Blood* Web site), further supporting that the *Ptpn11*-mutant microenvironment drives MPN development by hyperactivation of resident HSCs. Notably, the disrupted HSC cell-cycle distribution caused by the *Ptpn11*$^{E76K/+}$ mutation in the BM stromal cells was largely corrected, and the dormancy in HSCs was restored in *Ptpn11*$^{E76K/+}$*Prx1-Cre*$^{+}$*CCL3*$^{-/-}$ double-mutant mice (Figure 1G).

The robust effect of *CCL3* gene deletion on the MPN induced by the *Ptpn11*$^{E76K/+}$ mutation in the BM stromal cells strongly suggests that CCL3 is a key mediator for the leukemogenic effect of the microenvironmental *Ptpn11*$^{E76K/+}$ mutation. The fact that depletion of the *CCL3* gene is more potent than pharmacological inhibition of CCL3 signaling[8] in mitigating the MPN driven by the *Ptpn11*-mutated microenvironment further supports this notion. These mouse genetic data combined with our previous pharmacological inhibition data[8] provide a clear mechanism for the detrimental effects of *Ptpn11*-activating mutations in the stem-cell microenvironment and suggest CCL3 as a therapeutic target for controlling leukemic progression in Noonan syndrome and for improving stem-cell transplantation therapy in Noonan syndrome–associated leukemias, especially considering that CCL3 itself is dispensable for normal hematopoiesis. Nevertheless, because both genetic and pharmacological approaches involve systemic effects, additional studies are required to determine the effects of stromal-cell type–specific deletion of CCL3 on microenvironmental *Ptpn11* mutation–induced leukemogenesis.

The online version of this article contains a data supplement.

Acknowledgments: This work was supported by National Institutes of Health, National Heart, Lung, and Blood Institute grant HL130995 (C.-K.Q.) and National Institutes of Health, National Institute of Diabetes and Digestive and Kidney Diseases grant DK092722 (C.-K.Q.).

Contribution: L.D. and H.Z. generated microenvironmental cell type–specific knockin mice and analyzed myeloproliferative neoplasm development/progression and hematopoietic stem cell phenotypes; C.-K.Q. designed the experiments and directed the entire project; and L.D. and C.-K.Q. wrote the manuscript.

Conflict-of-interest disclosure: The authors declare no competing financial interests.

Correspondence: Cheng-Kui Qu, Division of Hematology/Oncology/BMT, Department of Pediatrics, Aflac Cancer and Blood Disorders Center, Emory University School of Medicine, 1760 Haygood Dr NE, HSRB E302, Atlanta, GA 30322; e-mail: cheng-kui.qu@emory.edu.

References

1. Mohi MG, Neel BG. The role of Shp2 (PTPN11) in cancer. *Curr Opin Genet Dev*. 2007;17(1):23-30.
2. Tartaglia M, Mehler EL, Goldberg R, et al. Mutations in PTPN11, encoding the protein tyrosine phosphatase SHP-2, cause Noonan syndrome. *Nat Genet*. 2001; 29(4):465-468.
3. Roberts AE, Allanson JE, Tartaglia M, Gelb BD. Noonan syndrome. *Lancet*. 2013;381(9863):333-342.
4. Araki T, Mohi MG, Ismat FA, et al. Mouse model of Noonan syndrome reveals cell type- and gene dosage-dependent effects of Ptpn11 mutation. *Nat Med*. 2004;10(8):849-857.

Figure 1. Leukemogenic effects of the *Ptpn11*$^{E76K/+}$ mutation in the stem-cell microenvironment is abolished in *Ptpn11*$^{E76K/+}$ *Prx1-Cre*$^{+}$ *CCL3*$^{-/-}$ mice. (A) White blood cell counts in the peripheral blood (PB) of *Ptpn11*$^{E76K/+}$*Prx1-Cre*$^{+}$*CCL3*$^{-/-}$, *Ptpn11*$^{E76K/+}$*Prx1-Cre*$^{+}$, *CCL3*$^{-/-}$, and *Ptpn11*$^{+/+}$*Prx1-Cre*$^{+}$ mice (n = 5 mice per group) were determined at the indicated ages. (B-G) *Ptpn11*$^{E76K/+}$*Prx1-Cre*$^{+}$*CCL3*$^{-/-}$, *Ptpn11*$^{E76K/+}$*Prx1-Cre*$^{+}$, *CCL3*$^{-/-}$, and *Ptpn11*$^{+/+}$*Prx1-Cre*$^{+}$ mice were sacrificed at age 12 to 17 months. Spleen weights were documented (n = 7 mice per group) (B). Mac-1^{+}Gr-1^{hi} cells in the BM, spleen, liver, lung, and PB (n = 7 mice per group for BM, spleen, liver, and lung; n = 5 mice per group for PB) (C left), Mac-1^{+}Gr-1^{low} cells in the BM (n = 7 mice per group) (C right), and CD115^{+}Gr-1^{low} cells in the BM, spleen, liver, lung, and PB (n = 7 mice per group for BM, spleen, liver, and lung; n = 5 mice per group for PB) (D) were determined. Femurs, spleens, livers, and lungs were processed for histopathological examination (hematoxylin and eosin staining; n = 3 mice per group). Representative pictures are shown (E). The pool size of HSCs (Lin^{-}Sca-1^{+}c-Kit^{+} CD150^{+}CD48^{-}Flk2^{-}) in the BM (n = 7 mice per group) (F), and the cell-cycle distribution of HSCs in the BM (n = 7 mice per group) (G) were determined by multiparameter fluorescence-activated cell sorting. Data shown are mean ± standard deviation of all mice examined. $^{**}P < .01$; $^{***}P < .001$.

5. Xu D, Liu X, Yu WM, et al. Non-lineage/stage-restricted effects of a gain-of-function mutation in tyrosine phosphatase Ptpn11 (Shp2) on malignant transformation of hematopoietic cells. *J Exp Med*. 2011;208(10): 1977-1988.
6. Chan G, Kalaitzidis D, Usenko T, et al. Leukemogenic Ptpn11 causes fatal myeloproliferative disorder via cell-autonomous effects on multiple stages of hematopoiesis. *Blood*. 2009;113(18):4414-4424.
7. Mohi MG, Williams IR, Dearolf CR, et al. Prognostic, therapeutic, and mechanistic implications of a mouse model of leukemia evoked by Shp2 (PTPN11) mutations. *Cancer Cell*. 2005;7(2):179-191.
8. Dong L, Yu WM, Zheng H, et al. Leukaemogenic effects of Ptpn11 activating mutations in the stem cell microenvironment. *Nature*. 2016;539(7628):304-308.
9. Méndez-Ferrer S, Michurina TV, Ferraro F, et al. Mesenchymal and haematopoietic stem cells form a unique bone marrow niche. *Nature*. 2010; 466(7308):829-834.
10. Kunisaki Y, Bruns I, Scheiermann C, et al. Arteriolar niches maintain haematopoietic stem cell quiescence. *Nature*. 2013;502(7473): 637-643.
11. Cook DN, Beck MA, Coffman TM, et al. Requirement of MIP-1 alpha for an inflammatory response to viral infection. *Science*. 1995;269(5230): 1583-1585.
12. Logan M, Martin JF, Nagy A, Lobe C, Olson EN, Tabin CJ. Expression of Cre recombinase in the developing mouse limb bud driven by a Prxl enhancer. *Genesis*. 2002;33(2):77-80.

DOI 10.1182/blood-2017-06-791103

To the editor:

Circulatory and maturation kinetics of human monocyte subsets in vivo

Tamar Tak,[1] Julia Drylewicz,[2] Lennart Conemans,[1] Rob J. de Boer,[3] Leo Koenderman,[1] José A. M. Borghans,[2,*] and Kiki Tesselaar[2,*]

[1]Department of Respiratory Medicine and [2]Department of Immunology, Laboratory of Translational Immunology, University Medical Centre Utrecht, Utrecht, The Netherlands; and [3]Bioinformatics/Theoretical Biology, Utrecht University, Utrecht, The Netherlands

Monocytes originate from the bone marrow (BM), are distributed in the bloodstream, and can differentiate in the tissue into skin macrophages or intestinal dendritic cells (DCs).[1] They play an essential role in the defense against pathogens[2] and are implicated in a range of diseases.[3]

Labeling experiments with 6,6-$^2H_2$-glucose[4] and ^{3}H-thymidine[5,6] have suggested a monocyte residence time in blood of 2 to 4 days. Although these experiments considered monocytes as a single population, the currently held view is that at least 3 monocyte subsets exist: classical $CD14^{++}CD16^{-}$ monocytes (CMs), intermediate $CD14^{++}CD16^{+}$ monocytes (IMs), and nonclassical $CD14^{+}CD16^{++}$ monocytes (NCMs). The residence times of these subsets in blood and their interrelationship remain to be determined. The 3 subsets are characterized by the gradually changing expression of surface markers,[7] differential gene enhancer profiles[8] expression profiles,[9,10] and differences in functionality.[3,11] Their maturation kinetics also differ, because human CMs repopulate the bloodstream first after hematopoietic stem cell transplantation, followed by IMs and later by NCMs.[12] In rhesus macaques, similar results were found by using in vivo bromodeoxyuridine labeling.[13] The gradually changing expression patterns, combined with their consecutive repopulation/labeling kinetics has led to the prevailing idea that monocytes differentiate from CMs via IMs to NCMs.[9,13]

In mice, there is more direct evidence for such a linear differentiation pattern.[14] Adoptively transferred CM homologs were shown to differentiate into NCMs,[15,16] and in vivo imaged monocytes were shown to lose CM marker CCR2 while acquiring NCM marker CXC_3CR1 at sites of sterile inflammation.[17] However, adoptively transferred CM preparations might contain small numbers of monocyte progenitors[15] and thus, even in mice, there remains discussion on the developmental relation of these monocyte subsets under homeostatic conditions.[3,15,18]

To investigate the circulatory and maturation/differentiation kinetics of the human monocyte subsets, we used in vivo 6,6-$^2H_2$-glucose labeling in 14 volunteers[19,20] (see supplemental Methods, available on the *Blood* Web site). This study was performed after receiving approval from the local ethics review board (Medisch Ethische Toetsingscommissie Utrecht) and obtaining written informed consent from all volunteers in accordance with the Declaration of Helsinki. Our study population consisted of 5 healthy volunteers and 9 eosinophilic asthma patients. Because no differences in monocyte subset counts or labeling kinetics were found between asthma patients and healthy volunteers (supplemental Figure 1), we combined data from both groups for analysis.

Monocyte subset numbers and percentages in blood (Figure 1) were in agreement with previous findings,[3] with a median of 89% CMs, 4% IMs, and 7% NCMs. DNA ^{2}H-enrichment was first detected in CMs, in which it peaked at days 3 to 4, similar to earlier labeling studies on the whole monocyte compartment.[4,5] In IMs and NCMs, label enrichment was detected later and peaked after approximately 4 and 8 days, respectively. These findings are in line with previous results suggesting a linear differentiation pattern.[12,13]

Mathematical models (supplemental Methods) were fitted to the measured ^{2}H-enrichment levels to estimate monocyte subset kinetics. These models take into account the observed ratios between cell numbers in each subset (assumed to be constant) and assume that incorporation of label occurred only at the monocyte progenitor stage in the BM. After maturation in the postmitotic pool (PMP), the models assume that cells enter the bloodstream as CMs and subsequently mature into IMs and NCMs. Assuming differentiation from IMs into NCMs directly in the circulation gave reasonable fits to the enrichment data of CMs and IMs but failed to describe the delay with which label was observed in NCMs (Figure 2A). We therefore extended the model by assuming that IMs can mature into NCMs only after a delay of Δ_2 days, Assuming that this maturation step occurs inside the blood gave an improved fit to the data (Figure 2B; moderate improvement according to the Kullback-Leibler's scale; supplemental Methods), but an even better fit was obtained when we assumed that this differentiation step occurs outside the blood (Figure 2C).

For all models, we found 2 optima, 1 with slow and 1 with fast dynamics of BM precursors. The estimated average maturation time